Sensing and Bio-Sensing Research 50 (2025) 100871

Contents lists available at ScienceDirect

Sensing and Bio-Sensing Research

journal homepage: www.elsevier.com/locate/sbsr

Multivariate diagnostics of electrochemical sensor drift by in situ impedance spectroscopy and voltammetry: A benzenediol-based framework

Abhilash Krishnamurthy [a,b,*], Kristina Žagar Soderžnik [a,b]

[a] Department for Nanostructured Materials, Jožef Stefan Institute, Jamova cesta 39, 1000 Ljubljana, Slovenia
[b] Jožef Stefan International Postgraduate School, Jamova cesta 39, 1000 Ljubljana, Slovenia

ARTICLE INFO

Keywords:
Electrochemical impedance spectroscopy (EIS)
Screen-printed electrode (SPE)
Benzenediols
Sensor diagnostics
Equivalent circuit modelling
Multivariate analysis

ABSTRACT

Performance drift in electrochemical sensors remains a challenge in long-term and/or corrosive applications. We present a generalisable, in situ diagnostic framework based on electrochemical impedance spectroscopy (EIS) and cyclic voltammetry (CV), using screen-printed electrodes (SPE) and benzenediols (catechol, resorcinol and hydroquinone) in acidic media as a model system. Two sensor types, unmodified and Pt/C-modified SPEs, were tested across repeated CV cycles, with polarisation resistance (R_P) and effective capacitance (C_{eff}) extracted from equivalent circuit models.

Unmodified SPEs showed progressive activation, while modified SPEs exhibited early improvement followed by degradation. To synthesise trends across R_P, C_{eff}, and net charge transfer (Q_n) obtained from CV data, principal component analysis (PCA) was applied. PCA revealed smooth, directional evolution for unmodified SPEs and disordered, non-monotonic drift in modified SPEs, reinforcing the EIS results.

This approach enables online, non-destructive tracking of electrochemical sensor health and offers a transferable framework for performance assurance, quality control, and lifecycle monitoring. It repositions EIS from static characterisation to an embedded, multivariate diagnostic tool.

1. Introduction

Growing public concern over "Sick Building Syndrome" [1] (SBS) has driven the rapid development of sensors for detecting volatile toxic organic compounds [2] (VTOC), which can accumulate to hazardous levels and cause both acute and chronic illnesses. The scientific community has addressed this need by developing sensors capable of detecting and quantifying VTOCs (e.g., benzene, formaldehyde [3]) with low detection limits and rapid, near real-time response [4]. Electrochemical sensing [5] is particularly well-suited to this task, offering selectivity, sensitivity, and speed [6] in both gas and liquid phases. It also offers a cost-effective alternative to optical [7] or calorimetric methods [8].

Electrochemical sensors are prone to performance drift when exposed to environmental stressors such as electrolyte [9] variation, analyte interaction, and corrosive media. These conditions alter reaction kinetics and compromise sensor integrity [10], especially during trace analyte detection [11] or extended operation under harsh conditions. Over time, such drift reduces the sensor's operational reliability and lifespan [12].

Conventional methods such as scanning electron microscopy (SEM) [13], energy-dispersive X-ray spectroscopy (EDXS) [14], X-ray photoelectron spectroscopy (XPS) [15], surface-enhanced Raman spectroscopy (SERS) [16], and X-ray diffraction (XRD) [17] offer valuable insights into material degradation. However, they are destructive, equipment-intensive, and require specialised training, making them impractical for routine diagnostics.

Electrochemical impedance spectroscopy (EIS) [18] offers a viable, non-destructive diagnostic alternative. It can sensitively track surface changes such as corrosion [19] or nucleation [20] without damaging the sensor. Because redox processes are directly linked to the electrochemically active surface area [21], EIS provides an effective means of evaluating sensor performance.

In this study, we diagnose performance drift in screen-printed electrodes (SPEs) by monitoring their electrical properties using periodic in situ EIS measurements. EIS spectra recorded at multiple time points were compared to track changes, and equivalent electrical circuits were fitted to assess the evolution of circuit elements. EIS is used here not as a post-modification tool but as an integrated diagnostic protocol embedded in the sensing workflow. This enables online health

* Corresponding author at: Department for Nanostructured Materials, Jožef Stefan Institute, Jamova cesta 39, 1000 Ljubljana, Slovenia.
E-mail address: abhilash.krishnamurthy@ijs.si (A. Krishnamurthy).

https://doi.org/10.1016/j.sbsr.2025.100871
Received 25 June 2025; Received in revised form 18 August 2025; Accepted 1 September 2025
Available online 2 September 2025

monitoring and offers a transferable framework adaptable across sensor types and analytes. Two sets of Metrohm DS150 electrodes were tested: one unmodified and one with the working electrode (WE) modified by drop-casting a 20 wt% Pt/C suspension [platinum nanoparticles (2–3 nm) on Vulcan XC-72R]. EIS spectra were recorded before and after cyclic voltammetry (CV) with three different benzenediol isomers [catechol (CC), resorcinol (RS) and hydroquinone (HQ)] in 1 M HCl. Building on our previous article in *Electrochimica Acta* (Krishnamurthy et al., 2024) [22], which demonstrated the viability of the modified SPE-based sensing platform and detailed the benzenediol redox mechanisms, we retain CC, RS, and HQ as model analytes due to their well-studied, reproducible electrochemistry. For the electrolyte, we employ 1 M HCl, also as discussed in the previous article, to suppress spontaneous oxidation and to decrease solution resistance, thereby providing a stable measurement matrix for the present analysis. The results confirm that EIS is an effective tool for assessing surface condition and sensor health [23]. While benzenediols served as model analytes, the framework is generalisable to other molecular classes. This work quantifies sensor performance evolution using impedance-derived metrics that are applicable across architectures. Fig. 1 illustrates the EIS-based characterisation process applied to both unmodified and Pt/C-modified SPEs.

2. Principles and modelling frameworks in electrochemical impedance spectroscopy

EIS is a powerful technique for probing the resistive and capacitive behaviour of electrochemical systems across a wide frequency range. In this study, we interpret EIS spectra using equivalent circuit models that represent key physical and electrochemical processes at the electrode–electrolyte interface.

Fig. 2 presents representative Nyquist, Bode, and complex capacitance plots with fitted curves from the equivalent circuit model. While Nyquist and Bode plots are traditionally used in control systems [24] to assess cut-off frequencies and system stability, our focus here is on circuit fitting and the evolution of electrical parameters. These plots therefore serve mainly as fitting tools rather than standalone diagnostic aids. Full datasets, theoretical background, and symbolic circuit diagrams (Supplementary Figs. S1–S4) are provided in the Supplementary Information.

2.1. Optimising equivalent circuits for mechanistic interpretation

Selecting an equivalent circuit [25] requires balancing completeness with interpretability. Over-modelling can yield near-perfect fits but risks introducing elements without clear electrochemical justification. Under-modelling, while sacrificing fit quality, ensures that each element corresponds to a physically meaningful process. In this work, we prioritised the latter approach to maintain mechanistic clarity. Diffusion-related components were excluded, as the SPE setup lacks controlled mass transport (e.g., flow systems or rotating electrodes). The simplified circuit thus emphasises clarity and interpretability over exhaustiveness.

3. Results and discussion

3.1. Extracting mechanistic insight from equivalent circuit analysis

EIS spectra were obtained to compare:

1. The performance of unmodified versus Pt/C-modified DS150 SPEs.
2. The evolution of unmodified SPE performance over baseline, post-five, and post-ten CV cycles.
3. The evolution of Pt/C-modified SPEs over the same cycling intervals.

EIS data were fitted using a modified Randles' circuit (Fig. 3), which

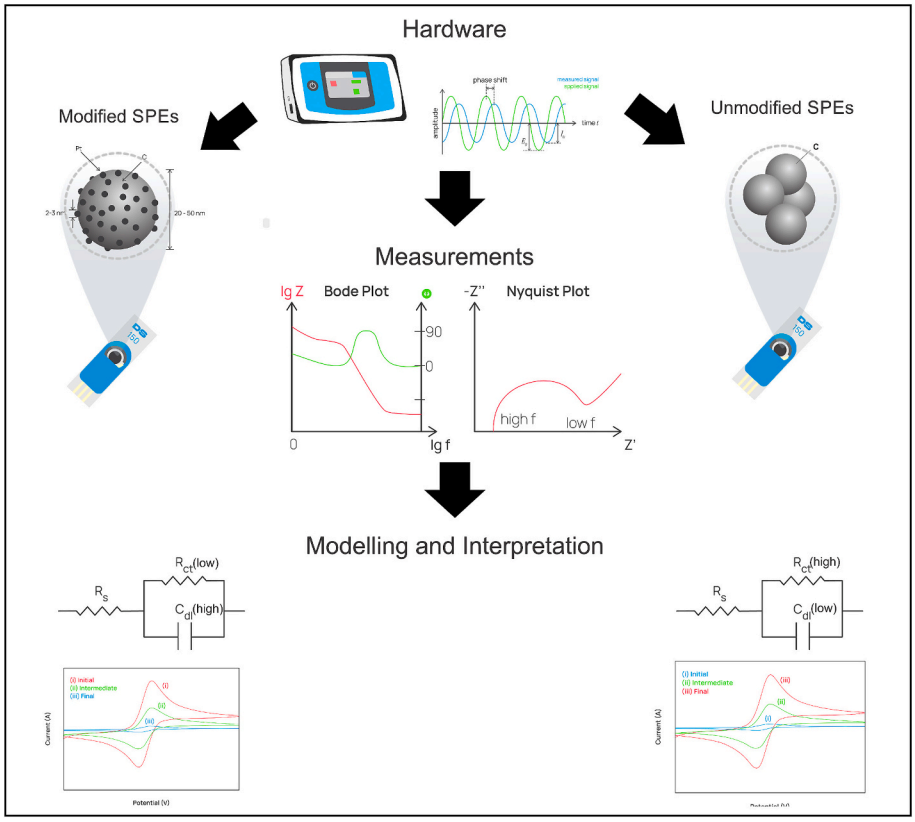

Fig. 1. (Graphical abstract): Schematic of the in situ EIS-based diagnostic workflow for SPEs. Impedance measurements yield R_P and C_{eff} as online, non-invasive indicators of sensor performance drift and degradation across unmodified and Pt/C-modified electrodes.

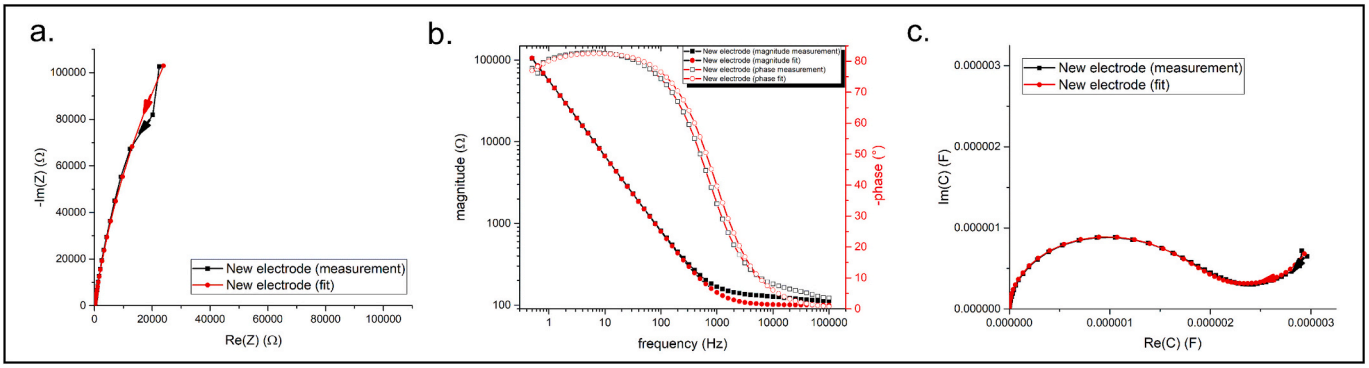

Fig. 2. EIS characterisation of an SPE in 1 M HCl, showing experimental data (black) and fitted model (red, $\chi^2 = 0.0020$). Plots include (a) Nyquist, (b) Bode, and (c) complex capacitance. Data were fitted using a Randles' circuit incorporating a constant phase element (CPE) to account for non-ideal double-layer behaviour. (For interpretation of the references to colour in this figure legend, the reader is referred to the web version of this article.)

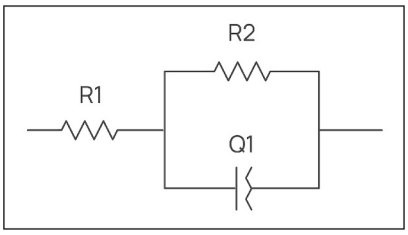

Fig. 3. Modified Randles' equivalent circuit used for EIS fitting. The model includes solution resistance (R1), polarisation resistance (R2), and a constant phase element (Q1) to account for non-ideal capacitive behaviour.

includes solution resistance (R_S), polarisation resistance (R_P), and a constant phase element (CPE) in place of an ideal capacitor to account for non-ideal capacitive [26] behaviour (see Supplementary Section 1.3.3). Mass transport effects were excluded, as they introduce additional elements (e.g., Warburg impedance [27]) that, while physically meaningful, complicate interpretation. By focusing on resistive and capacitive components, the model preserves mechanistic clarity. Each EIS dataset corresponds to a single SPE and reflects its individual condition.

We extracted values for solution resistance R_S (R1, Ω), polarisation resistance R_P (R2, Ω), and the CPE parameters T and ϕ, as defined in Supplementary Eqs. S12–S15. These parameters describe non-ideal double-layer capacitance. From these, we calculated the effective capacitance C_{eff} (F) [28], which we interpret as a diagnostic indicator of double-layer behaviour and surface integrity, using the following formula:

$$C_{eff} = T^{\frac{1}{\phi}}\left(\frac{1}{R_S} + \frac{1}{R_P}\right)^{\frac{(\phi-1)}{\phi}} \quad (1)$$

Supplementary Figs. S5–S13 show Nyquist, Bode, and complex capacitance plots for each condition, with one representative replicate displayed for clarity. Full fitted data from the EIS spectra are provided in Supplementary Tables S1–S9.

3.2. Translating electrical response into diagnostic indicators of sensor performance

3.2.1. Impedance-based comparison of unmodified and Pt/C-modified SPEs

Before evaluating the effects of sensor use on SPE performance, we first examined whether Pt/C modification [29] altered the electrodes' baseline electrochemical response. EIS measurements were performed on both unmodified and modified SPEs in 1 M HCl, as summarised in Table 1.

Table 1
Impedance parameters (R_P, C_{eff}) for unmodified and Pt/C-modified SPEs in 1 M HCl.

Parameter	R_P (kΩ)	C_{eff} (μF)
Unmodified SPE	900.00	1.75
Modified SPE	13.00	90.51

We assessed the impact of Pt/C modification using R_P and C_{eff} as key diagnostic indicators. Lower impedance values typically indicate enhanced electrochemical performance [30]. Following modification, R_P decreased while C_{eff} increased significantly. The rise in C_{eff} reduces capacitive reactance, consistent with their inverse relationship (see Eq. S8 in Supplementary Section 1.3.2). These shifts are substantial: R_P reduced by a factor of approximately seventy, and C_{eff} increased by nearly a factor of fifty. Because solution resistance (R_S) depends mainly on electrolyte concentration, which remained constant at 1 M HCl, it was not a primary comparison metric in this study.

3.2.2. Impedance-based performance tracking of unmodified SPEs during cyclic voltammetry

We evaluated the performance of unmodified SPEs under CV in four analyte solutions: 1 M HCl (blank), 1 mM CC, 1 mM RS and 1 mM HQ, all in 1 M HCl. For each analyte, EIS spectra were recorded at three stages: before cycling, after five cycles, and after ten cycles. These measurements were used to track changes in R_P and C_{eff}. Table 2 presents the corresponding circuit element values.

The unmodified SPEs exhibited a decrease in R_P and an increase in C_{eff} over successive cycles. This trend indicates surface activation and improved sensor response under corrosive conditions. It likely reflects electrochemical polishing [31], removing surface films and exposing more conductive substrate material [32]. These observations are consistent with previous reports of electrochemical carbon oxidation in acidic media [33].

3.2.3. Impedance-based performance tracking of Pt/C-modified SPEs during cyclic voltammetry

We conducted a parallel investigation using Pt/C-modified SPEs, following the same protocol applied to unmodified SPEs (Section 3.2.2). Table 3 summarises the circuit element values derived from EIS measurements in HCl, CC, RS, and HQ.

Similar to the unmodified SPEs, the Pt/C-modified counterparts showed consistent trends in R_P and C_{eff}. However, a key distinction emerged: in all four analytes, C_{eff} increased after five cycles but declined by the tenth. For R_P, a general increase was observed from baseline to ten cycles, except with resorcinol, where R_P decreased. These trends suggest that Pt/C-modified SPEs undergo transient improvement,

Table 2
Impedance evolution (R_P, C_{eff}) for unmodified SPEs at baseline, five and ten CV cycles in blank (1 M HCl), catechol, resorcinol, and hydroquinone.

Analyte	Blank		Catechol		Resorcinol		Hydroquinone	
Parameter	R_P (kΩ)	C_{eff} (μF)	R_P (kΩ)	C_{eff} (μF)	R_P (kΩ)	C_{eff} (μF)	R_P (kΩ)	C_{eff} (μF)
Baseline	900.00	1.80	2000.00	1.54	1700.00	2.28	1000.00	1.86
Post-five cycles	300.00	4.30	700.00	3.30	500.00	4.62	200.00	6.69
Post-ten cycles	180.00	5.70	300.00	4.10	350.00	5.11	100.00	11.65

Table 3
Impedance evolution (R_P, C_{eff}) for Pt/C-modified SPEs at baseline, five and ten CV cycles in blank (1 M HCl), catechol, resorcinol, and hydroquinone.

Analyte	Blank		Catechol		Resorcinol		Hydroquinone	
Parameter	R_P (kΩ)	C_{eff} (μF)	R_P (kΩ)	C_{eff} (μF)	R_P (kΩ)	C_{eff} (μF)	R_P (kΩ)	C_{eff} (μF)
Baseline	13.00	90.51	16.00	71.41	20.00	57.78	10.00	85.32
Post-five cycles	15.00	111.61	13.00	108.79	20.00	86.71	11.00	110.60
Post-ten cycles	18.00	77.44	18.00	95.10	17.00	77.40	15.00	82.13

followed by degradation, as reflected in the shifts in R_P and C_{eff}. The modified SPEs appear to maintain stable electrical characteristics for up to five cycles, after which degradation becomes evident. This likely results from Pt nanoparticle dissolution [34], carbon support oxidation, and agglomeration, all of which accelerate in acidic media [35] [36]. These effects reduce the electrochemically active surface area and alter the impedance profile over time [37]. Given the initial sharp decline in R_P and the rise in C_{eff} after modification, even modest catalyst loss could significantly impact performance, especially considering the low catalyst loading (~10 μg per SPE). These impedance-based findings were supported by complementary CV data, which revealed early signs of surface deterioration during operation.

Fig. 4 visually consolidates the impedance trends: unmodified electrodes improved progressively with CV cycling, while modified electrodes degrade post-five cycles. This divergence in log-scaled R_P and C_{eff} highlights EIS's strength in capturing early behavioural shifts, without relying on fixed performance thresholds. Logarithmic (base-10) scaling accommodates the wide dynamic range of R_P and C_{eff} across cycles.

Table 4 summarises parameter shifts and relative standard deviations (RSD) across cycling stages, providing comparative insight into performance trends. Unmodified SPEs showed large changes in R_P and C_{eff}, but with high variability. In contrast, Pt/C-modified electrodes exhibited smaller but more consistent changes: R_P generally increased, and C_{eff} peaked at five cycles before declining by ten. The lower RSDs in the modified electrodes indicate greater reproducibility. These results

Table 4
Summary of impedance parameter evolution over ten CV cycles for unmodified and Pt/C-modified SPEs.

Parameter	Metric	Unmodified SPE	Pt/C-modified SPE
R_P	Δ 0 → 5 cycles (%)	−65.50	12.10
	Δ 5 → 10 cycles (%)	2.60	20.10
	Δ 0 → 10 cycles (%)	−64.60	34.40
	Rate (%/cycle)	−6.460	3.44
	RSD (0–10 cycles) (%)	93.40	15.90
C_{eff}	Δ 0 → 5 cycles (%)	138.90	26.50
	Δ 5 → 10 cycles (%)	−4.60	−22.00
	Δ 0 → 10 cycles (%)	128.00	−1.30
	Rate (%/cycle)	12.80	−0.13
	RSD (0–10 cycles) (%)	51.20	19.00

Metrics include percentage changes, rate of drift, relative standard deviation (RSD), and coefficient of variation (CoV).

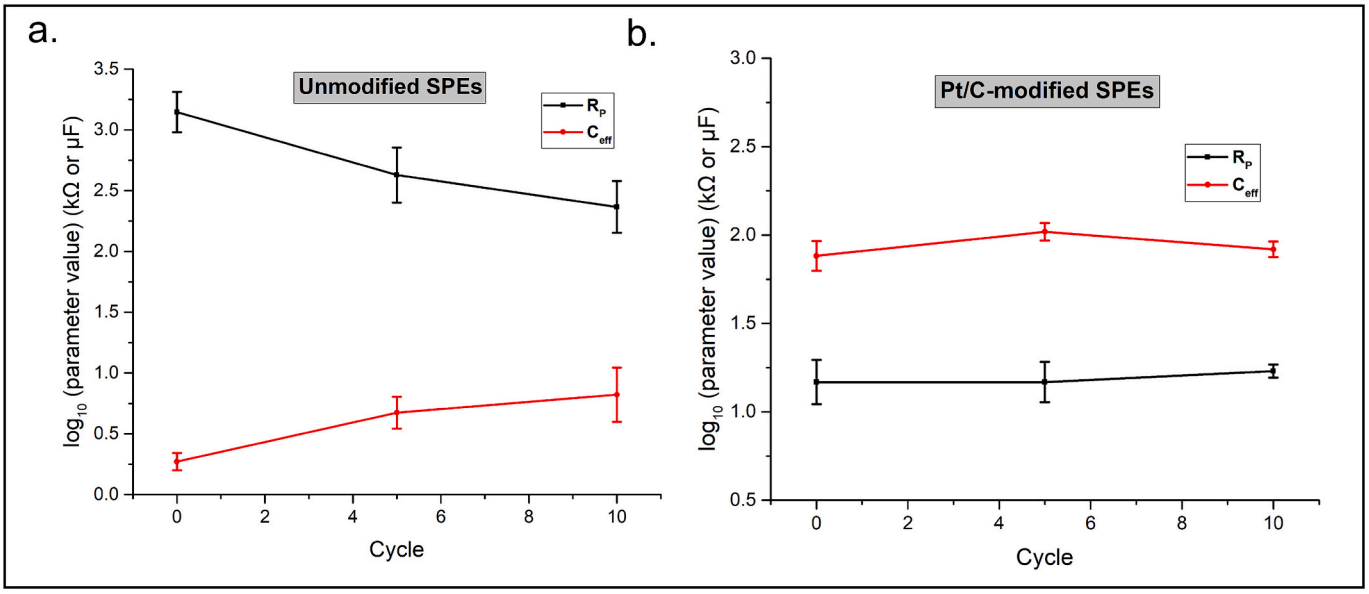

Fig. 4. Logarithmically-scaled evolution of polarisation resistance (R_P) and effective capacitance (C_{eff}) across baseline, five and ten CV cycles for (a) unmodified and (b) Pt/C-modified SPEs. Trends serve as diagnostic indicators of improvement in unmodified electrodes and degradation onset in modified specimens. Error bars show intra-analyte variability and confirm trend consistency.

suggest that surface modification not only improves consistency but also influences the trajectory of sensor drift, reinforcing the sensitivity of the proposed impedance-based diagnostic framework.

Trends in R_P and C_{eff} provide insight into sensor precision and stability, complementing traditional performance metrics such as limit of detection (LoD) and linearity. These impedance-derived indicators are particularly well-suited for long-term deployment and for ensuring metrological robustness.

3.3. Cross-validation of impedance metrics via cyclic voltammetry

We analysed CV data to corroborate the conclusions drawn from EIS. Since all measurements used a fixed CV window, differences in current magnitude or redox onset reflect variations in sensor responsiveness. Fig. 5 presents CV data in 1 M HCl from three representative experimental sets, based on the protocols outlined in Section 3.1.

Fig. 5a shows that Pt/C-modified SPEs produce higher current responses than unmodified electrodes, likely reflecting enhanced H^+ adsorption on the Pt [38] surface. This observation aligns with the impedance-based findings of lower R_P and higher C_{eff} following modification. Fig. 5b and c illustrate performance evolution over CV cycles: unmodified electrodes exhibit gradual improvement, whereas modified electrodes show an initial increase followed by a decline, consistent with the EIS trends. These patterns validate the circuit parameters derived from EIS.

Supplementary Figs. S14–S16 present the relevant CV plots for each experimental condition, with one representative replicate shown per condition for clarity and brevity.

CV data were used to extract key descriptors of electrochemical performance, including net charge transferred (Q_n), peak separation (ΔE_P), and their evolution over successive cycles. Q_n indicates the extent of redox activity, while ΔE_P reflects the reversibility and efficiency of electron transfer. These parameters help distinguish the two SPE types in terms of catalytic behaviour and stability. Pt/C-modified electrodes exhibited better kinetics, as shown by narrower ΔE_P and lower onset potentials, but also displayed signs of degradation over time, particularly with resorcinol, which is prone to fouling. In contrast, unmodified electrodes showed slower but more consistent redox behaviour, with either stable or slightly increasing charge transfer over repeated cycling. These results suggest that while the unmodified carbon surface is initially less active, it provides more stable diagnostic behaviour over time. By comparison, Pt/C modification enhances initial performance but reduces durability. Table 5 summarises these trends. Definitions and complete CV parameters are provided in Supplementary Section 1.5 and Tables S10–S17.

Tables 4 and 5 provide complementary evidence from EIS and CV, respectively. Together, they confirm both qualitative and quantitative shifts in performance, reinforcing the diagnostic potential of the proposed methodology. Notably, EIS detects subtle changes in sensor behaviour before degradation becomes apparent in CV data. These trends reflect the progressive, cycle-dependent evolution of the electrode surface.

Table 5
Summary of cyclic voltammetry parameters for unmodified and Pt/C-modified SPEs, showing net charge transfer (Q_n), peak separation (ΔE_P), and their evolution across cycles.

SPE Type	Analyte	Q_n Range (μC)	ΔE_P (mV)	Q_n Trend	Interpretation
Unmodified	HCl	7.9–25.3	–	↑	Minimal activity; non-faradaic blank system
	HQ	233–261	180 → 150	↑ (+28 μC)	Progressive activation and stable redox reversibility
	CC	239–243	200 → 210	Stable	Consistent performance, minor improvement
	RS	97.9 → 3.8	–	↓ (−94 μC)	Rapid degradation due to polymerisation
Pt/C-modified	HCl	115–167	–	↓ (−51 μC)	Some signal drift; potential surface evolution
	HQ	236–264	60	↑ (+28 μC)	Sustained catalytic activity; gradual drift in Q_{pn}
	CC	261–344	60 → 70	↑ (+83 μC)	Strong catalytic response with stable reversibility
	RS	147 → 101	–	↓ (−46 μC)	Partial degradation; initial performance then decline

3.4. Principal component analysis of electrochemical drift

To complement the impedance and voltammetric analyses, we applied principal component analysis (PCA) to visualise the evolution of sensor behaviour across CV cycles. PCA was performed on three descriptors: R_P, C_{eff}, and Q_n. Separate analyses were conducted for unmodified and Pt/C-modified SPEs, capturing the distinct diagnostic trajectories of each platform. Fig. 6 shows the two PCA biplots for unmodified and Pt/C-modified SPEs.

For unmodified SPEs, the first two principal components (PC1 and PC2) accounted for 92.1 % of total variance (PC1 = 56.8 %, PC2 = 35.3 %). The PCA scores plot revealed smooth, directional shifts with increasing cycles, especially in HCl and HQ, consistent with progressive surface activation. Feature loadings indicated that PC1 was dominated

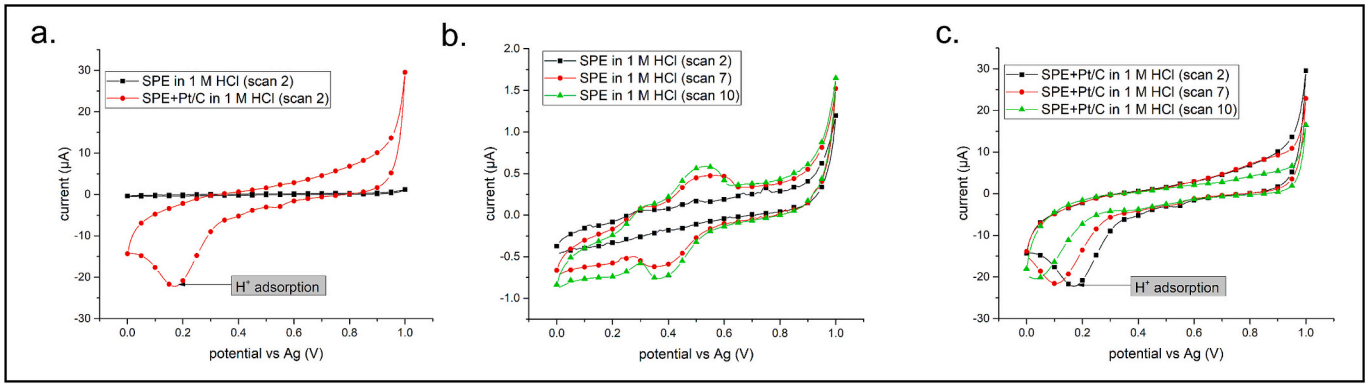

Fig. 5. CV data for SPEs in 1 M HCl across 0–1 V vs quasi Ag reference at 10 mV s^{-1}. (a) Pt/C-modified electrodes exhibit higher current response compared to unmodified SPEs. (b) Unmodified electrodes show progressive performance shifts with cycling. (c) Modified electrodes demonstrate initial improvement, followed by decline after extended cycling.

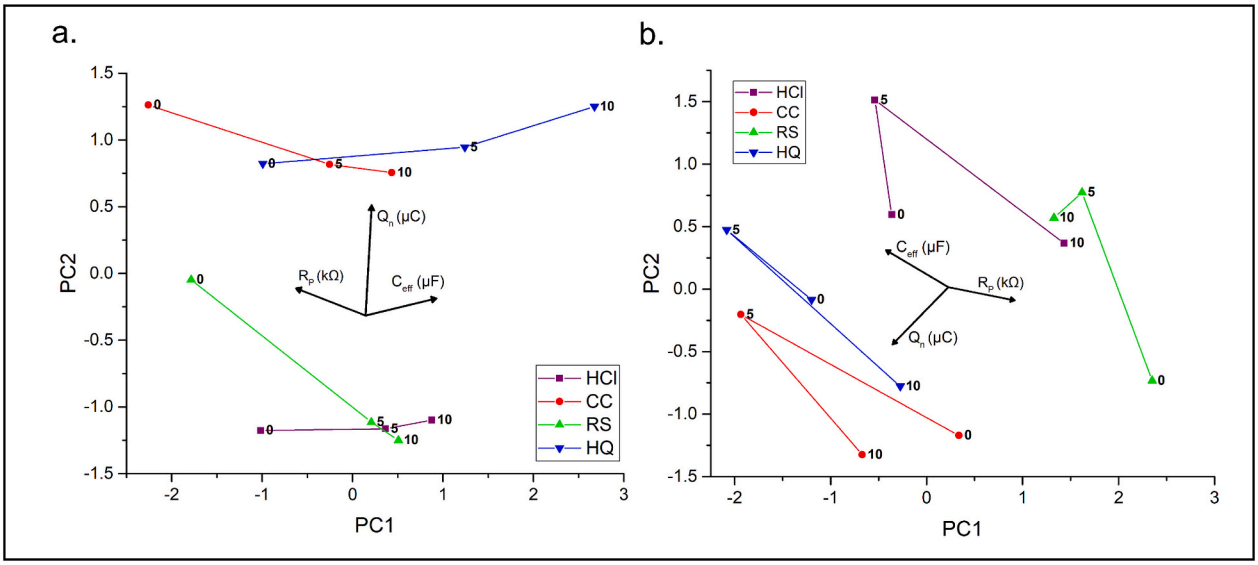

Fig. 6. PCA of SPE performance across CV cycles based on R_P, C_{eff}, and Q_n. (a) Unmodified SPEs show clear, cycle-dependent progression. (b) Pt/C-modified SPEs exhibit scattered behaviour consistent with degradation.

by inverse trends in R_P and Q_n, while PC2 captured secondary contributions from C_{eff}. This supports the interpretation that sensor improvement over time results from simultaneous resistive and capacitive enhancement.

In contrast, Pt/C-modified SPEs exhibited more scattered behaviour. The first two components explained 88.4 % of variance (PC1 = 54.6 %, PC2 = 33.8 %), but progression between cycles was less structured. The PCA biplot showed that C_{eff} and Q_n still influenced PC1 most strongly, but the vector directions were less aligned, reflecting the non-monotonic degradation observed experimentally. In particular, electrodes modified with Pt/C exhibited increasing R_P but decreasing C_{eff} after five to ten cycles, which disrupted the directional trend visible in unmodified electrodes.

Together, the PCA results reinforce the notion that unmodified carbon SPEs undergo consistent electrochemical activation, whereas Pt/C-modified SPEs have a limited peak performance window due to catalyst degradation. The dimensionality reduction confirms that R_P, C_{eff}, and Q_n are sufficient to track sensor health in reduced space, offering a potential framework for automated or embedded diagnostics.

3.5. Synthesis of impedance and voltammetric trends

To consolidate the trends observed across all experimental conditions, Table 6 summarises the evolution of R_P and C_{eff} for both unmodified and Pt/C-modified SPEs across each analyte after five and ten CV cycles.

Table 6
Summary of qualitative R_P and C_{eff} trends for unmodified and Pt/C-modified SPEs across all analytes post-five and ten CV cycles.

SPE Type	Analyte	Post five cycles	Post ten cycles	Observation from CV
Unmodified	HCl HQ CC RS	$R_P \downarrow, C_{eff} \uparrow$	$R_P \downarrow, C_{eff} \uparrow$	*Consistent improvement in diagnostic indicators*
Pt/C-modified	HCl	$R_P \uparrow, C_{eff} \uparrow$	$R_P \uparrow, C_{eff} \downarrow$	*Emerging signs of degradation*
	HQ	$R_P \downarrow, C_{eff} \uparrow$		
	CC	$R_P -, C_{eff} \uparrow$	$R_P \downarrow, C_{eff} \downarrow$	
	RS			

Arrows indicate parameter changes; qualitative observations describe performance evolution.

cycles. The table highlights directional changes, allowing straightforward comparison of performance evolution during cycling.

Trends observed in both EIS and CV data suggest that acidic corrosion, rather than analyte-specific redox reactions, is the primary driver of changes in electrode surface state and impedance parameters. While CV captures broader behavioural changes, EIS offers higher-resolution, quantitative insight and allows direct comparison to baseline conditions. This underscores the value of using EIS alongside complementary techniques for comprehensive sensor evaluation.

4. Applications and prospects

A key advantage of this method is its ability to assess SPE health and performance in situ, without removing the sensor from operation. Unlike SEM, SERS, XPS, or XRD, which require disassembly and interrupt sensing, this approach enables continuous, non-invasive diagnostics. This work redefines the role of EIS in sensing applications. In traditional sensor studies, EIS is used only as a static characterisation tool, limited to Nyquist plots recorded before and after modification. By contrast, our method integrates EIS directly into the sensing workflow, enabling online diagnostic tracking. Monitoring R_P and C_{eff} over time allows the framework to identify degradation and distinguish between charge transfer loss and capacitive drift. This shifts EIS from a passive characterisation method to an active performance assurance tool. Potential applications include quality control during sensor fabrication, predictive maintenance in environmental or biomedical systems, and embedded diagnostics in portable devices. Although this diagnostic strategy appears scalable, the trends reported here are specific to DS150 SPEs and may not directly generalise to other platforms. Extending the framework to additional systems is a key focus of ongoing work. This positions EIS not just as an analytical method but as a foundation for intelligent sensor design and lifecycle management.

5. Scope and limitations

Due to the complexity of the dataset, which includes Nyquist, Bode, and complex capacitance plots at three stages (baseline, post-five cycles, and post-ten cycles) across four analytes in triplicate, we present only representative spectra for clarity. Trends within each analyte were reproducible across replicates, as illustrated by the error bars in Fig. 4. These margins reflect intra-condition variability and demonstrate

consistent directional changes, though they do not imply statistical significance. Directional trends in R_P and C_{eff} were observed across all four analytes: three redox-active and one non-faradaic, the former serving as functional replicates. This approach enabled internal validation while preserving the variability characteristic of commercial SPEs. Batch-to-batch variability among SPEs limited the comparability of baseline impedance values, as reflected in the high RSDs for unmodified electrodes shown in Table 4. For modified electrodes, additional variability arose from the manual drop-casting process, which, despite careful technique, introduced inconsistencies in catalyst deposition. These factors contributed to fluctuations in fitted parameters and complicated direct comparison across samples. Each SPE effectively served as an individual case study, with fabrication variation, surface morphology, and catalyst distribution driving unique electrochemical responses. As such, the absolute values of the fitted parameters are less critical than their evolution within a given sample across cycles. Reproducibility was established through protocol repetition across multiple analytes, all of which exhibited consistent directional trends. This approach prioritises mechanistic interpretation and trend validation over inter-sample averaging.

As discussed in Section 3.2, while EIS effectively characterises and investigates the electrical behaviour of SPEs, the underlying phenomena responsible for the observed changes in parameter values remain to be confirmed. SEM provides the most direct means of validating these findings, allowing examination before and after CV cycling. However, since SEM sample preparation is destructive, it precludes further electrochemical testing on the same SPE. SERS, with its high surface sensitivity similar to EIS, could potentially validate the impedance data under a robust test protocol. Nonetheless, SERS also typically requires destructive sample preparation, precluding comparative before-and-after measurements on the same SPE. Another potential solution involves employing an electrochemical quartz crystal microbalance (EQCM) [39] to monitor changes in resonant frequency during CV cycling. However, this approach necessitates the development of a suitable method to integrate the SPE with the EQCM electrode. Alternatively, we could assess material erosion [40] by depositing a proxy layer on the EQCM electrode and extrapolating the results to the SPE, while carefully considering the subtle differences between the two systems.

6. Conclusion

In situ electrochemical impedance spectroscopy (EIS) was used to characterise screen-printed electrodes (SPE) by modelling them as networks of discrete circuit elements. We diagnosed performance drift in both unmodified and Pt/C-modified SPEs using periodic EIS measurements taken before and after sensing. The impedance spectra were fitted using a Randles' circuit, with a constant phase element (CPE) replacing the ideal capacitor to account for non-ideal double-layer behaviour. From these fits, we extracted polarisation resistance (R_P) and effective capacitance (C_{eff}) as diagnostic indicators. Modification reduced R_P and increased C_{eff}, confirming enhanced baseline performance with Pt/C deposition. Both electrode types were evaluated using cyclic voltammetry (CV) with four analytes: 1 M HCl (blank), 1 mM catechol, 1 mM resorcinol, and 1 mM hydroquinone in 1 M HCl. EIS spectra were recorded at three points: before cycling, after five cycles, and after ten cycles. Unmodified SPEs showed progressive improvements in impedance characteristics, indicating increased electrochemical activity over time. In contrast, modified SPEs displayed initial improvement followed by degradation, suggesting loss of catalytic integrity. These trends, supported by CV results, confirm the reliability of R_P and C_{eff} as indicators of surface condition and sensor drift. Although demonstrated with benzenediols, this diagnostic approach is generalisable to other molecular systems and sensing platforms. The proposed framework offers a modular strategy for tracking sensor performance and positions EIS as a foundational tool for intelligent lifecycle management of electrochemical systems.

7. Materials and methods

7.1. Catalyst preparation

Catalyst ink was prepared by dispersing 20 wt% Pt/C [platinum nanoparticles (2–3 nm) on Vulcan XC-72R (20–50 nm), sourced from FuelCellStore] in 0.995 ml of absolute ethanol. A 5 µl aliquot of 5 % Nafion solution (in ethanol, Sigma Aldrich) was added as a binder. The mixture was ultrasonicated using a 500 W probe at 25 % amplitude for 2 min to ensure uniform dispersion. The ink was used immediately to minimise particle settling and agglomeration.

7.2. Sensor element fabrication

Sensor elements were prepared using Metrohm DropSens DS150 SPEs with a carbon working electrode (WE), platinum counter electrode (CE), and silver reference electrode (RE). The WE was cleaned with deionised water and ethanol, then dried on a 55 °C hot plate. A 10 µl aliquot of catalyst ink was pipetted onto the WE while still on the hot plate to accelerate drying. Care was taken to avoid spill-over onto the CE and RE. The sensors were stored in a sealed, dry container to prevent tarnishing of the RE and silver contacts. Each 10 µl ink dose contained 10 µg of catalyst (1 mg/ml), with 20 % Pt, resulting in a metal loading of 2 µg per sensor and an estimated Pt loading of approximately 160 ng mm^{-2} for a 4 mm WE diameter.

7.3. Analyte solution preparation

Analyte solutions of various concentrations were prepared by diluting stock solutions of each benzenediol. Catechol (CC), resorcinol (RS) and hydroquinone (HQ), all of analytical grade purity (>99 %) and purchased from Sigma Aldrich, were used. Stock solutions of each benzenediol (50 mM) were created by dissolving the analyte in 1 M HCl (prepared by dilution of 37 % HCl) with stirring, aided by ultrasonication. Working solutions were prepared by diluting the stock with 1 M HCl to reach target concentration. For each measurement, 75 µl of analyte solution was dispensed onto the SPE surface to ensure full coverage of all three electrodes.

7.4. Framework summary

This protocol integrates EIS into the sensing workflow to track sensor performance over time. The steps are as follows:

7.4.1. Baseline measurement

Record EIS on a freshly prepared sensor to extract initial R_P and C_{eff} values.

7.4.2. Electrochemical cycling - Phase I

Perform x cycles of CV, followed by stabilisation.

7.4.3. Midpoint assessment

Measure EIS again and compare results to the baseline to observe early trends.

7.4.4. Cycling - Phase II

Apply another x CV cycles (total $2x$) and allow the system to stabilise.

7.4.5. Post-cycling measurement

Conduct a third EIS measurement and evaluate parameter evolution across 0, x, and $2x$ cycles.

7.4.6. Data interpretation

Compute % change and RSD for R_P and C_{eff}. Track directional trends to differentiate charge transfer shifts and capacitive changes.

7.4.7. Extension (Optional)

Repeat as needed for extended diagnostics. In this study, $x = 5$ cycles was used to capture early- and mid-stage sensor behaviour.

7.5. Electrochemical measurement protocols and data fitting

CV was performed using a PalmSens4 potentiostat with the following parameters: E_{begin} = 0 V, $E_{vertex1}$ = 1 V, $E_{vertex2}$ = 0 V vs quasi Ag reference; Scan rate: 10 mV s^{-1}; Number of scans: 10; Potential step size: approximately 1 mV. EIS was also performed using the PalmSens4 potentiostat under the following conditions: Equilibration time: 0 s; Scan Type: Default; DC potential (E_{dc}): 0 V; AC amplitude (E_{ac}): 10 mV (rms); Frequency type: Scan; Number of frequencies: 54 (10 per decade); Maximum frequency: 100 kHz; Minimum frequency: 0.5 Hz; Minimum sampling time: 0.5 s; Maximum equilibration time: 10 s.

Equivalent circuit fitting used non-linear least squares regression. For the representative dataset shown in Fig. 2, the model yielded a reduced χ^2 value of 0.0020, indicating excellent agreement between experimental data and the fitted response. Similar fit quality was observed across all datasets used for performance tracking.

Funding

This research was supported by the Slovenian Research Agency (ARIS) under grants P2–0084, J2–1739, J2–3051, and PR-09874.

Ethical approval

Not applicable.

CRediT authorship contribution statement

Abhilash Krishnamurthy: Writing – review & editing, Writing – original draft, Visualization, Validation, Methodology, Investigation, Formal analysis, Data curation, Conceptualization. **Kristina Žagar Soderžnik:** Writing – review & editing, Validation, Supervision, Resources, Project administration, Methodology, Investigation, Funding acquisition.

Declaration of competing interest

The authors declare no competing interests.

Acknowledgements

The authors gratefully acknowledge the Slovenian Research Agency (ARIS) for their financial contribution to this work provided through grants: P2–0084 (Programme Nanostructured Materials), J2–1739 (High Performance Nanostructured Acrylamide Sensors), J2-3051 (SensePMC), and PR-09874 (Young Researcher Project). The authors also thank Pika Štefančič for her assistance with the graphical artwork.

Appendix B. Supplementary data

While we generated a comprehensive collection of EIS plots, we provide it as supplementary material to ensure the main article remains concise. The supplement also includes a detailed theoretical overview of electrochemical impedance spectroscopy (EIS), including explanations of key electrical circuit elements such as resistors, capacitors, and constant phase elements (CPEs), along with symbolic representations and derivations. Supplementary data to this article can be found online at [https://doi.org/10.1016/j.sbsr.2025.100871].

Data availability

All data supporting the findings of this study are available within the article and its Supplementary Information. Additional datasets can be provided by the corresponding author upon reasonable request.

References

[1] C.A. Redlich, J. Sparer, M.R. Cullen, Sick-building syndrome, Lancet 349 (9057) (1997) 1013–1016.
[2] S.K. Brown, M.R. Sim, M.J. Abramson, C.N. Gray, Concentrations of volatile organic compounds in indoor air–a review, Indoor Air 4 (2) (1994) 123–134.
[3] Š. Trafela, A. Krishnamurthy, K.Ž. Soderžnik, U. Kavčič, I. Karlovits, B. Klopčič, K. Žužek, IoT electrochemical sensor with integrated Ni (OH) 2–Ni nanowires for detecting formaldehyde in tap water, Sensors 23 (10) (2023) 4676.
[4] R. Mall, Real-Time Systems: Theory and Practice, Pearson Education India, 2009.
[5] A. Hayat, J.L. Marty, Disposable screen printed electrochemical sensors: tools for environmental monitoring, Sensors 14 (6) (2014) 10432–10453.
[6] M.J. Tierney, H.O.L. Kim, Electrochemical gas sensor with extremely fast response times, Anal. Chem. 65 (23) (1993) 3435–3440.
[7] C. Elosua, I.R. Matias, C. Bariain, F.J. Arregui, Volatile organic compound optical fiber sensors: a review, Sensors 6 (11) (2006) 1440–1465.
[8] B. Szulczyński, J. Gębicki, Currently commercially available chemical sensors employed for detection of volatile organic compounds in outdoor and indoor air, Environments 4 (1) (2017) 21.
[9] N. Govindarajan, A. Xu, K. Chan, How pH affects electrochemical processes, Science 375 (6579) (2022) 379–380.
[10] E.E. Stansbury, R.A. Buchanan, Fundamentals of electrochemical corrosion, ASM Int. (2000).
[11] E.S. Cross, L.R. Williams, D.K. Lewis, G.R. Magoon, T.B. Onasch, M.L. Kaminsky, J. T. Jayne, Use of electrochemical sensors for measurement of air pollution: correcting interference response and validating measurements, Atmos. Meas. Tech. 10 (9) (2017) 3575–3588.
[12] E. Demir, K.K. Kırboga, M. Işık, An overview of stability and lifetime of electrochemical biosensors, Novel Nanostruct. Mater. Electrochem. Bio-sens. Appl. (2024) 129–158.
[13] W. Zhou, R. Apkarian, Z.L. Wang, D. Joy, Fundamentals of scanning electron microscopy (SEM), Scann. Microsc. Nanotechnol. (2007) 1–40.
[14] D. Shindo, T. Oikawa, D. Shindo, T. Oikawa, Energy dispersive x-ray spectroscopy, Anal. Electron Microsc. Mater. Sci. (2002) 81–102.
[15] J. Chastain, R.C. King Jr., Handbook of X-ray photoelectron spectroscopy, Perkin-Elmer Corp. 40 (221) (1992) 25.
[16] P.L. Stiles, J.A. Dieringer, N.C. Shah, R.P. Van Duyne, Surface-enhanced Raman spectroscopy, Annu. Rev. Anal. Chem. 1 (2008) 601–626.
[17] J. Epp, X-ray diffraction (XRD) techniques for materials characterization, in: Materials Characterization Using Nondestructive Evaluation (NDE) Methods, Woodhead Publishing, 2016, pp. 81–124.
[18] B.Y. Chang, S.M. Park, Electrochemical Impedance Spectroscopy, Annu. Rev. Anal. Chem. 3 (1) (2010) 207–229.
[19] D.V. Ribeiro, J.C.C. Abrantes, Application of electrochemical impedance spectroscopy (EIS) to monitor the corrosion of reinforced concrete: a new approach, Constr. Build. Mater. 111 (2016) 98–104.
[20] C.X. Wang, M. Wang, X. Zhou, Nucleation and growth of apatite on chemically treated titanium alloy: an electrochemical impedance spectroscopy study, Biomaterials 24 (18) (2003) 3069–3077.
[21] A. García-Miranda Ferrari, C.W. Foster, P.J. Kelly, D.A. Brownson, C.E. Banks, Determination of the electrochemical area of screen-printed electrochemical sensing platforms, Biosensors 8 (2) (2018) 53.
[22] A. Krishnamurthy, Z. Samardžija, Š. Trafela, A. Korent, S. Šturm, K.Ž. Soderžnik, Electrochemical detection of benzenediols using carbon-supported catalysts, Electrochim. Acta 493 (2024) 144389.
[23] F. Arduini, F. Di Nardo, A. Amine, L. Micheli, G. Palleschi, D. Moscone, Carbon black-modified screen-printed electrodes as electroanalytical tools, Electroanalysis 24 (4) (2012) 743–751.
[24] G.F. Franklin, J.D. Powell, A. Emami-Naeini, Feedback Control of Dynamic Systems vol. 10, Pearson, Upper Saddle River, NJ, 2010.
[25] A.J. Bard, L.R. Faulkner, H.S. White, Electrochemical Methods: Fundamentals and Applications, John Wiley & Sons, 2022.
[26] B.B. Damaskin, O.A. Petrii, Historical development of theories of the electrochemical double layer, J. Solid State Electrochem. 15 (2011) 1317–1334.
[27] J. Huang, Diffusion impedance of electroactive materials, electrolytic solutions and porous electrodes: Warburg impedance and beyond, Electrochim. Acta 281 (2018) 170–188.
[28] B. Hirschorn, M.E. Orazem, B. Tribollet, V. Vivier, I. Frateur, M. Musiani, Determination of effective capacitance and film thickness from constant-phase-element parameters, Electrochim. Acta 55 (21) (2010) 6218–6227.
[29] G. Paimard, E. Ghasali, M. Baeza, Screen-printed electrodes: fabrication, modification, and biosensing applications, Chemosensors 11 (2) (2023) 113.
[30] N.O. Laschuk, E.B. Easton, O.V. Zenkina, Reducing the resistance for the use of electrochemical impedance spectroscopy analysis in materials chemistry, RSC Adv. 11 (45) (2021) 27925–27936.
[31] G. Yang, B. Wang, K. Tawfiq, H. Wei, S. Zhou, G. Chen, Electropolishing of surfaces: theory and applications, Surf. Eng. 33 (2) (2017) 149–166.

[32] F. Nazneen, P. Galvin, D.W. Arrigan, M. Thompson, P. Benvenuto, G. Herzog, Electropolishing of medical-grade stainless steel in preparation for surface nano-texturing, J. Solid State Electrochem. 16 (2012) 1389–1397.
[33] Z. Siroma, M. Tanaka, K. Yasuda, K. Tanimoto, M. Inaba, A. Tasaka, Electrochemical corrosion of carbon materials in an aqueous acid solution, Electrochemistry 75 (2) (2007) 258–260.
[34] S. Mitsushima, Y. Koizumi, S. Uzuka, K.I. Ota, Dissolution of platinum in acidic media, Electrochim. Acta 54 (2) (2008) 455–460.
[35] N. Linse, L. Gubler, G.G. Scherer, A. Wokaun, The effect of platinum on carbon corrosion behavior in polymer electrolyte fuel cells, Electrochim. Acta 56 (22) (2011) 7541–7549.
[36] H. Tang, Z. Qi, M. Ramani, J.F. Elter, PEM fuel cell cathode carbon corrosion due to the formation of air/fuel boundary at the anode, J. Power Sources 158 (2) (2006) 1306–1312.
[37] M. Lee, M. Uchida, D.A. Tryk, H. Uchida, M. Watanabe, The effectiveness of platinum/carbon electrocatalysts: dependence on catalyst layer thickness and Pt alloy catalytic effects, Electrochim. Acta 56 (13) (2011) 4783–4790.
[38] F.G. Will, Hydrogen adsorption on platinum single crystal electrodes: I. Isotherms and heats of adsorption, J. Electrochem. Soc. 112 (4) (1965) 451.
[39] A.R. Hillman, The EQCM: electrogravimetry with a light touch, J. Solid State Electrochem. 15 (2011) 1647–1660.
[40] O. Schneider, An EQCM study of the corrosion of synthetic aluminium alloys, ECS Trans. 16 (52) (2009) 13.